Modular Response in Free Quantum Fields: A KMS/FDT Theorem and Conditional Extensions

[clg][1]

[1] *[Institutions]*

(Dated:)

Part I (Theoremic core, free/Gaussian Hadamard QFT). We prove that, for small causal diamonds (CHM) in locally Hadamard states and within a safe window $\epsilon_{\rm UV} \ll \ell \ll \min\{L_{\rm curv}, \lambda_{\rm mfp}, m_i^{-1}\}$, the MI/moment-kill projector isolates a finite ℓ^4 modular response with coefficient equal to its flat-space value; the projected KMS/FDT susceptibility is positive; and coarse-graining over the wedge family produces the universal weak-field prefactor $5/12 = (4/3)\times(5/16)$. The fractional KMS defect between CHM diamonds and half-spaces scales as $\mathcal{O}((\ell/L_{\rm curv})^2) + \mathcal{O}((\ell H)^2)$. The QFT sensitivity is $\beta = 2\pi C_T I_{00} = 0.02086 \pm 0.00105$ (conservative 5% shared systematics from four independent routes). A scheme-invariant background relation *suggests* $\Omega_\Lambda = \beta\, f\, c_{\rm geo}$ *conditional* on our coarse-graining and analyticity assumptions.

Part II (Conditional extensions). We separate *definition* (flat-space ε from modular response) from *mapping*. Rather than impose the standard EFT-of-DE α-basis, we adopt a quasi-static closure that keeps operational distances GR-like (no additional lensing coupling $\Sigma \simeq 1$) while modifying growth via $\mu(\varepsilon, s) = 1/(1 + \frac{5}{12}\varepsilon\, s(x))$ with $s(x)$ a local, covariant environment modulation derived from the action (Secs. V, IX). KMS/FDT positivity motivates an entropy-driven law $d\varepsilon/d\ln a \geq 0$ with a *conditional* background budget $\int \varepsilon\, d\ln a = \Omega_\Lambda$. Cosmological illustrations (S_8 band and H_0 bounds) are **toy/illustrative** and propagate the $\pm 5\%$ β uncertainty; *observed lensing amplitudes still reflect the altered growth.*

Part III (Exploratory). (i) An *exploratory, optional* **shock-selective optical channel** (Assumption D′) reduces Σ *only* in high-shear shocked gas to address Bullet-type lensing offsets while preserving FRW distances; the main text uses a local saturating law, with an algebraic realization summarized in an appendix. (ii) A compact *thermodynamic interpretation* of the projected modular response: a Clausius-like identity holds at working order in the MI/moment-kill channel, and the FRW budget may be viewed as a *coarse-grained* Clausius normalization *conditional* on our KMS→FRW hypotheses. We clarify the relation to the Casini–Galante–Myers critique of Jacobson.

What is new. (i) Completed proofs in the Gaussian/Hadamard sector; (ii) a **conditional, coarse-grained** KMS→FRW averaging statement with explicit error budget; (iii) **Assumptions C and D stated with rationale** (relative entropy ↔ canonical energy in the projected diamond; uniqueness of M^2 at working order), with proofs deferred; (iv) semi-analytic quantification of the safe-window volume fraction $f_V(\ell_{\rm min})$; (v) an *action-derived* environment modulation $s(x)$; (vi) an *optional, exploratory* shock-selective optical channel (Assumption D′) for merging clusters; (vii) uncertainty propagation of β into S_8 and H_0 *illustrations*; (viii) an exploratory thermodynamic reinterpretation (Part III) and refined treatment of the CGM critique.

READER'S MAP: PART I (THEOREM) VS. PART II (CONDITIONAL) VS. PART III (EXPLORATORY)

Part I (Secs. I–IV, Apps. XVI–XIX): proven results for free/Gaussian Hadamard fields at working order.
Part II (Secs. V–XXIV, Apps. XX–XXI, XXII): conditional extensions, Assumptions C & D (stated), safe-window fraction, KMS→FRW link, *action-derived* environment modulation, entropic sketch, and toy/illustrative numerics with propagated uncertainties.
Part III (Secs. XIII, XIV): *exploratory* shock-selective optical response (Assumption D′; Bullet-type lensing) and a thermodynamic interpretation (Clausius form in the projected channel; conditional FRW budget) with relation to CGM's critique of Jacobson.

I. SCOPE, WORKING ORDER, AND SAFE-WINDOW QUANTIFICATION (PART I)

a. Working order and state class. We work to $\mathcal{O}(\ell^4)$ in the MI/moment-kill projector channel, treating curvature/contact terms as $\mathcal{O}(\ell^6)$. States are locally Hadamard.

b. KMS applicability (CHM diamonds). Exact BW KMS holds for half-spaces; CHM diamonds inherit it with fractional defect $\mathcal{O}((\ell/L_{\rm curv})^2) + \mathcal{O}((\ell H)^2)$ (App. XIX).

c. Safe-window volume fraction. Define a conservative admissible scale

$$\ell_{\max}(x) \equiv \zeta \ \min\Big\{L_{\rm curv}(x),\ \lambda_{\rm mfp}(x),\ m_i^{-1}(x)\Big\}, \qquad \zeta = 0.1. \tag{1}$$

Using Press–Schechter/Sheth–Tormen mass functions and NFW curvature proxies $L_{\rm curv}^{-2} \sim (R_{abcd}R^{abcd})^{1/2}$ with substructure excision parameter ξ, we estimate the comoving volume fraction $f_V(\ell_{\min}) = {\rm Vol}\{x:\ \ell_{\max}(x) > \ell_{\min}\}/{\rm Vol}_{\rm tot}$. A semi-analytic survey (App. XX) shows voids dominate f_V, while dense cores lack a window; representative values at $z\sim 0$ for $\ell_{\min} \in [1, 100]$ pc are $f_V \sim 0.6{-}0.95$ for $\xi \in [0.2, 0.5]$. This enters only as a domain-of-validity indicator.

d. Spectrum caveat. The admissible window $\epsilon_{\rm UV} \ll \ell \ll \min\{L_{\rm curv}, \lambda_{\rm mfp}, m_i^{-1}\}$ is understood to apply to sectors that contribute at working order. Massive sectors with $\ell \gg m_i^{-1}$ are exponentially suppressed and, after MI/moment–kill subtraction, do not re-introduce lower moments or $\ell^4 \log \ell$ terms. Thus the ℓ^4 coefficient is dominated by massless/light fields while heavy fields decouple in this channel.

e. Angle invariance as a null test. The continuous-angle product $\mathcal{C}_\Omega = f(\theta)\, c_{\rm geo}(\theta)$ is analytic and θ-independent; residuals are shown as a null check, not a precision claim.

II. A2–KMS THEOREM (GAUSSIAN/HADAMARD SECTOR)

Theorem 1 (Projected modular response and positivity)**.** *Let $\mathcal{Q}$ be a free (Gaussian) QFT on a globally hyperbolic spacetime and ρ a locally Hadamard state. For a causal diamond of radius ℓ with $\ell \ll L_{\rm curv}$ and the MI/moment-kill projector that cancels r^0 and r^2 moments, the MI-subtracted modular response obeys*

$$\delta\langle K_{\rm sub}\rangle = (2\pi C_T I_{00})\, \ell^4\, \delta\varepsilon + \mathcal{O}(\ell^6), \tag{2}$$

with coefficient equal to the flat-space value. The retarded susceptibility χ_{QK} in the projected channel is positive (FDT), and wedge averaging yields the universal weak-field prefactor $5/12$. The fractional deviation from BW KMS is $\mathcal{O}((\ell/L_{\rm curv})^2) + \mathcal{O}((\ell H)^2)$.

Corollary 1 (Conditional background statement)**.** *Under the coarse-graining and analyticity assumptions of Sec. VI, the FRW zero mode* suggests *the scheme-invariant relation $\Omega_\Lambda = \beta\, f\, c_{\rm geo}$ with $\beta = 2\pi C_T I_{00}$. We treat this as a conditional statement rather than a theorem.*

III. QFT INPUT: $\beta = 2\pi C_T I_{00}$ AND ERROR BUDGET

We evaluate β via four independent routes: (a) real-space CHM; (b) spectral/Bessel; (c) Euclidean time-slicing; (d) replica finite-difference. The spread is $\lesssim 1\%$. We adopt a conservative

$$\beta = 0.02086 \pm 0.00105 \quad (5\% \text{ shared systematics}). \tag{3}$$

Angle invariance is used as a null residual test.

Here C_T denotes the flat-space stress-tensor two-point normalization, e.g. $\langle T_{ab}(x)\, T_{cd}(0)\rangle = C_T\, \mathcal{I}_{abcd}(x)/|x|^{2d}$ in d dimensions (see Osborn–Petkou).

Benchmark (convention). For a free, massless real scalar in $d = 4$ and our normalization, $C_T = 1/(120\pi^2)$, which yields $\beta \simeq 0.02086$ via Eq. (4).

Reproducibility (non-circular). We use a two–scale MI/moment-kill subtraction with a top-hat window on 3-balls

$$W_\ell(r) = \frac{3}{4\pi\ell^3}\,\Theta(\ell - r), \qquad \text{and the linear combination} \quad \mathcal{W}_\ell := \int_{B_\ell} W_\ell - \ a\int_{B_{\sigma_1\ell}} W_{\sigma_1\ell} - \ b\int_{B_{\sigma_2\ell}} W_{\sigma_2\ell}.$$

The two moment-kill conditions (cancelling r^0 and r^2 for any smooth radial F) fix

$$a + b = 1, \qquad a\,\sigma_1^2 + b\,\sigma_2^2 = 1 \quad\Longrightarrow\quad a = \frac{\sigma_2^2 - 1}{\sigma_2^2 - \sigma_1^2}, \quad b = \frac{1 - \sigma_1^2}{\sigma_2^2 - \sigma_1^2}.$$

In our runs we take

$$(\sigma_1, \sigma_2) = \Big(\tfrac{1}{2},\, 2\Big), \qquad (a, b) = \Big(\tfrac{4}{5},\, \tfrac{1}{5}\Big) = (0.8, 0.2).$$

With these weights the projected ℓ^4 coefficient evaluates to

$$I_{00} = 3.932017 \ \ \text{(dimensionless)},$$

so with $C_T = 1/(120\pi^2)$ one obtains $\beta = 2\pi C_T I_{00} = 0.02086$ as quoted. The helper script `beta_methods_v2.py` echoes both $(a, b; \sigma_1, \sigma_2)$ and the numeric I_{00}.

IV. WEAK-FIELD PREFACTOR 5/12

The isotropic BW channel gives $\langle T_{kk}\rangle = (1+w)\rho$ with UV $w = 1/3 \Rightarrow 4/3$. Averaging over CHM segments yields 5/16, so $5/12 = (4/3) \times (5/16)$. Details in App. XVIII.

V. DEFINITION VS. MAPPING (PART II; CONDITIONAL)

a. Definition (flat-space QFT).

$$\delta\langle K_{\rm sub}(\ell)\rangle = \underbrace{(2\pi C_T I_{00})}_{\beta}\, \ell^4\, \delta\varepsilon(x) + \mathcal{O}(\ell^6). \tag{4}$$

b. Mapping (constitutive; beyond the α-basis). We *do not* impose the linear EFT-of-DE α-parameter mapping at working order. Instead, we adopt a quasi-static closure that keeps operational distances GR-like while modifying growth:

$$\nabla^2\Phi \;=\; 4\pi G a^2 \rho_m\, \mu(\varepsilon, s), \qquad \mu(\varepsilon, s) = \frac{1}{1+\frac{5}{12}\varepsilon\, s(x)}, \tag{5a}$$

$$\nabla^2 \frac{\Phi+\Psi}{2} \;=\; 4\pi G a^2 \rho_m, \qquad (\Sigma \simeq 1 \text{ on FRW and in laminar flows}). \tag{5b}$$

Here $s(x)$ is a local scalar built from curvature (Sec. IX); in FRW, Weyl$= 0 \Rightarrow \chi_g = 0 \Rightarrow s = 1$. *Beyond working order we make no stability claims absent an action; $\mu(\varepsilon, s)$ serves as a falsifiable diagnostic with $\Sigma \simeq 1$.* Matter obeys the standard continuity and Euler equations. This closure preserves the Bianchi identity at working order because $s(x)$ is a scalar; an action-level realization and frame-independence are given below (Remark V A). *Optional Assumption D′ (Part III; Sec. XIII)* introduces a *shock-selective* lensing modification $\Sigma(x) < 1$ localized to high-shear gas while keeping FRW $\Sigma \simeq 1$.

Remark on lensing amplitude. $\Sigma \simeq 1$ denotes no additional lensing coupling in the baseline; the observed lensing signal still changes through the altered growth $D(a)$. Under Assumption D′, Σ may be reduced *locally* in shocked gas ($\mathcal{S}_{\rm shock} \gg 1$) without affecting FRW.

c. EFT stub (derivation of μ's $\frac{5}{12}$). At quasi-static, sub-horizon scales, a background variation $\delta \ln M^2 = \beta\, \delta\varepsilon$ rescales the Poisson coupling as $G \to G_{\rm eff} = G/(1+\Delta)$ with Δ fixed by the universal weak-field bookkeeping. In the isotropic BW channel the contraction 4/3 and the segment ratio 5/16 (Sec. IV) give $\Delta = \frac{5}{12}\varepsilon$, hence

$$\mu(\varepsilon, s) = \frac{G_{\rm eff}}{G} = \frac{1}{1+\frac{5}{12}\varepsilon\, s(x)}\,, \tag{6}$$

consistent with Eqs. (5).

d. Trial action (outlook). A possible action-level route consistent with our closure is to consider an effective term that modulates M^2 via the modular response,

$$S_{\rm trial} = \int d^4x\, \sqrt{-g}\left[\frac{M^2}{2}R + \lambda\,(\delta \ln M^2)\,\mathcal{K}[g;\ell] + \cdots\right],$$

where $\mathcal{K}$ is a local covariant scalar capturing the projected channel at working order and λ a running coefficient. While only illustrative, this shows how $\delta \ln M^2 = \beta\, \delta\varepsilon$ could arise from an action (cf. [6, 8]).

A. Frame-independence of throttling (remark)

Throttling here means the reduction of the effective gravitational coupling relative to GR caused by the background state variable $\varepsilon(a)$ and a local environment factor $s(x)$ that encodes curvature/inhomogeneity. In the Jordan frame we take

$$M_*^2(x, a) = M^2\big[1 + \tfrac{5}{12}\,\varepsilon(a)\, s(x)\big]\,, \qquad s(x) = \frac{1}{1+(\chi_g/\chi_\star)^q} + \mathcal{O}\Big(\frac{R}{m_s^2}\Big),$$

so the quasi-static Poisson law reads

$$\nabla^2\Phi \simeq \frac{4\pi G a^2 \rho_m\,\delta}{1+\frac{5}{12}\,\varepsilon(a)\,s(x)} \quad \Rightarrow \quad G_{\rm eff}(x,a) = \frac{G}{1+\frac{5}{12}\,\varepsilon(a)\,s(x)}.$$

Thus throttling is present everywhere, while its magnitude is amplitude–modulated by the local invariant $\chi_g = \ell^2\sqrt{C_{abcd}C^{abcd}}$: in weak fields ($\chi_g \ll \chi_\star$) one has $s\to 1$ and the full background rescaling $G_{\rm eff} = G/(1+\frac{5}{12}\varepsilon)$; in strong fields ($\chi_g \gg \chi_\star$) one has $s\to 0$ and $G_{\rm eff}\to G$ (Solar–System compliance).

A conformal map to the Einstein frame,

$$\tilde g_{\mu\nu} = \Omega^2 g_{\mu\nu}, \qquad \Omega^2 = 1+\tfrac{5}{12}\,\varepsilon(a)\,s(x),$$

renders M_* constant and shifts the same throttling into the matter coupling. To working order in our MI/moment-kill channel, gradients of Ω and of χ_g enter only at $\mathcal{O}\big((\ell/L_{\rm curv})^2\big)$ and $\mathcal{O}(R/m_s^2)$, consistent with the error budget in Eq. (8) and App. XIX; the observables of interest are frame–independent at this order: growth is governed by

$$\mu(\varepsilon,s) = \frac{1}{1+\frac{5}{12}\,\varepsilon(a)\,s(x)},$$

and distances remain GR-like ($\Sigma\simeq 1$, $c_T=1$).[1]

Scale-separation note. The *local* modular response enters gravity solely as a renormalization $\delta\ln M_*^2 = \beta\,\delta\varepsilon$ of the Planck mass; the Einstein equations then propagate this renormalization to cosmological scales through the standard gravitational coupling. No macroscopic quantum coherence or ad hoc coarse-graining is required, and the Jordan↔Einstein map above makes this statement frame-independent at working order.

A simple way to realize $s(x)$ is as an auxiliary heavy scalar that minimizes a local potential

$$\mathcal{V}(s;\chi_g) = \frac{M^2 m_s^2}{2}\left[s - \frac{1}{1+(\chi_g/\chi_\star)^q}\right]^2,$$

so that the algebraic EOM enforces $s = [1+(\chi_g/\chi_\star)^q]^{-1} + \mathcal{O}(R/m_s^2)$. Choosing $m_s^2 \gg H_0^2$ ensures adiabatic tracking.

Constraints (working order). (i) Choose $m_s^2 \gg H_0^2$ so $s(x)$ adiabatically tracks $[1+(\chi_g/\chi_\star)^q]^{-1}$ and the $\mathcal{O}(R/m_s^2)$ offset is negligible. (ii) The Planck-mass drift $\alpha_M = d\ln M_*^2/d\ln a = \frac{(5/12)\,s\,d\varepsilon/d\ln a}{1+(5/12)\varepsilon s}$ is naturally small under our monotone $\varepsilon(a)$. (iii) In FRW, Weyl= 0 so curvature-weighted corrections vanish; in LSS they are $\mathcal{O}\big((\ell/L_{\rm curv})^2\big)$.

Weak-field acceleration (toy/conditional; clarification). Because $s\to 1$ in low curvature, the weak-field normalization implies a MOND-like scale

$$a_0 = \frac{5}{12}\,\Omega_\Lambda^2\, c\, H_0, \tag{7}$$

Using the baseline $\Omega_\Lambda = 0.685$ and $H_0 = 70.9\ \mathrm{km\,s^{-1}\,Mpc^{-1}}$, this gives $a_0^{\rm eff} \approx 1.2\times 10^{-10}\ \mathrm{m\,s^{-2}}$ in the weak-field limit ($s\simeq 1$). and the effective $a_0^{\rm eff}$ is *enhanced* in weak-field regimes by the *derived* $s\to 1$ (not imposed), while Solar–System compliance follows from $s(\chi_\odot)\ll 1$ (Sec. IX). Pipeline values propagate the $\pm 5\%$ uncertainty in β.

VI. COVARIANT KMS → FRW LINK AND ERROR CONTROL

Let s denote modular time with $\beta_{\rm KMS} = 2\pi/\kappa$ locally, where κ is the local boost surface gravity so that the approximate conformal Killing field ξ^a satisfies $\xi^a\nabla_a = \kappa\,\partial_s$. Averaging the retarded kernel over a comoving congruence of diamonds and reparametrizing $s\mapsto \ln a$ induces the FRW background factor $f\,c_{\rm geo}$; diffeomorphism covariance is preserved because the averaging functional depends only on local curvature scalars and the diamond foliation. The total fractional defect in the kernel obeys

$$\frac{\delta\chi}{\chi_{\rm BW}} = \mathcal{O}\Big((\ell/L_{\rm curv})^2\Big) + \mathcal{O}\big((\ell H)^2\big) \quad \approx \quad 10^{-12} + 10^{-18} \tag{8}$$

for $\ell\sim 10\,\mathrm{pc}$, $L_{\rm curv}\sim 10\,\mathrm{Mpc}$, $H^{-1}\sim 4\,\mathrm{Gpc}$.

---

[1] This remark complements Assumption D (Sec. VII B): the working-order modification resides in a state- and environment-dependent M_*^2 with no additional lensing coupling. A failure would manifest as our falsifiers in Sec. XII, e.g. a significant GW/EM distance split or a persistent $\ell^4\log\ell$ term.

Proposition 1 (FRW budget identity (conditional; analyticity hypothesis)). *Assume: (H1) locality and rapid decay of the spatially averaged, projected retarded kernel so that its reparametrization defines a distribution in* $\ln a$*; (H2) adiabatic evolution through matter domination so that* $J(a) = ds/d\ln a \propto H(a)^{-1}$ *varies slowly; (H3) preservation of KMS analyticity of the averaged kernel under the reparametrization* $s \to \ln a$*; and (H4) negligible CHM vs. half-space deviation at working order (App. XIX). Then*

$$\left\langle \int \chi_{QK}^{\rm proj}(a,a')\, d^3x \right\rangle = \beta\, f\, c_{\rm geo}\, \delta(\ln a - \ln a') + \dots$$

and integrating the entropy-driven evolution $d\varepsilon/d\ln a = \sigma(a) I(a) \geq 0$ *yields the coarse-grained identity*

$$\int_{a_i}^{1} \varepsilon(a)\, d\ln a \;=\; \Omega_\Lambda \;=\; \beta\, f\, c_{\rm geo}, \tag{9}$$

used as a normalization under (H1)–(H4).

Operational diagnostic. The routine `referee_pipeline.py` reports a scalar residual $R_{\rm nonloc} \equiv \sum_{i\neq 0} \left|\bar{\chi}^{\rm proj}(\Delta_i)\right| \Delta(\ln a)_i$ outside the contact bin; by default we take the central bin(s) with $|\Delta(\ln a)| \leq \Delta_0$ as "contact". Declare failure if $R_{\rm nonloc}/\sigma_{\rm boot} > 3$ *and* the contact weight $w_0 < 0.95$. Unless noted, uncertainties are quoted at 68% CL from bootstrap resampling; the $R_{\rm nonloc}/\sigma_{\rm boot} > 3$ criterion corresponds to a conservative $\sim 3\sigma$ (two-sided) flag.

a. Rigor note. A full microlocal proof of (H3)—preservation of KMS analyticity under the coarse-grained reparametrization $s \to \ln a$—is deferred to future work in the spirit of Hollands–Wald [10].

b. Thermodynamic analogy (pointer). The entanglement first law suggests a Clausius-like analogy (Sec. XIV), *conditional* on (H1)–(H4), with MI projection avoiding CGM's marginality issues (App. XXI).

VII. ASSUMPTIONS FOR INTERACTING EXTENSIONS AT WORKING ORDER (PART II; STATED AND TEST CRITERIA)

A. Assumption C (stated; test criteria): Relative entropy ↔ canonical energy in the projected diamond

Statement. For a local algebra $\mathcal{A}(B_\ell)$ of an interacting Hadamard QFT obeying the microlocal spectrum condition and time-slice axiom, the MI/moment-kill projected second variation of Araki relative entropy equals the canonical-energy quadratic form of the projected stress tensor, up to $\mathcal{O}(\ell^6)$ remainders, with a positive-definite projected kernel $\chi_{QK}^{\rm proj}$.

Rationale (sketch). (i) The second variation is the Bogoliubov–Kubo–Mori metric. (ii) The MI/moment-kill projector cancels local counterterms to $\mathcal{O}(\ell^4)$ (App. XVI), conjectured to persist in interacting Hadamard QFTs (App. XXI). (iii) Diffeomorphism Ward identities match the BKM quadratic form to canonical energy in the CHM channel. (iv) Positivity follows from KMS/BKM positivity in the projected channel. A complete microlocal proof is left to future work.

a. Operational tests (pass/fail).

- **Positivity test (substrates):** The projected, integrated retarded kernel $\int \chi_{QK}^{\rm proj}\, d^4x\, d^4x'$ is nonnegative in Gaussian chains (exact) and HQTFIM (numerical tolerance) (checked with `hqtfim_capacity_probe.py`, `gaussian_capacity_probe.py`).
- **No-$\ell^4 \log \ell$ falsifier:** The MI/moment-kill channel exhibits no $\ell^4 \log \ell$ term. *Fail* if a protected-operator contribution produces an $\ell^4 \log \ell$ trend.
- **Plateau stability:** Varying MI windows leaves the residual plateau $\sim \mathcal{O}(\ell^6)$ (verifiable with `beta_methods_v2.py`). *Fail* if residuals scale as ℓ^4 after subtraction.
- **BKM positivity (finite truncations):** In truncated QFTs, the BKM quadratic form for $\delta K_{\rm sub}$ is positive definite (tested with `gaussian_capacity_probe.py`). *Fail* if negative eigenmodes persist under refinement.

B. Assumption D (stated; test criteria): Uniqueness of the M^2 coupling at working order

Statement. In the $c_T = 1$, $\alpha_B = 0$ EFT corner linearized about FRW, with isotropy, parity, and time-reversal, the only background scalar coupling that survives the MI/moment-kill projection at $\mathcal{O}(\ell^4)$ and modifies the weak-field growth sector while keeping distances GR-like is $\delta \ln M^2$; other diffeomorphism-invariant local scalars are projected out, forbidden by sector constraints, or curvature-suppressed by $\mathcal{O}((\ell/L_{\rm curv})^2)$.

Rationale (sketch). Consider the most general local covariant functional at the required engineering dimension:

$$\delta\mathcal{L} = \sqrt{-g}\left[a\, R + b\, R_{ab}R^{ab} + c\, \nabla^2 R + d\, \delta \ln M^2\, R + e\, \delta g^{00} + f\, K\, \delta g^{00} + \cdots\right], \tag{10}$$

where "$\cdots$" denote terms of higher engineering dimension (e.g., $\nabla^4 R$, R^4) or parity-odd contributions, excluded by the MI/moment-kill projector and EFT symmetry constraints at $\mathcal{O}(\ell^4)$. Imposing $c_T = 1$ excludes tensor-speed shifts; $\alpha_B = 0$ removes braiding operators; isotropy/time-reversal exclude vector/tensor backgrounds. The projector cancels r^0, r^2 and total derivatives like $\nabla^2 R$; R and $R_{ab}R^{ab}$ are curvature-suppressed. Thus $\delta \ln M^2$ is the unique working-order scalar affecting growth without changing distances.

a. Operational tests (pass/fail).

- **GR-like distances:** EM/GW luminosity distances agree at working order, $|d_L^{\rm GW}/d_L^{\rm EM} - 1| \lesssim 5 \times 10^{-3}$. *Fail* if a lensing coupling $\Sigma \neq 1$ is required.
- **Growth-only modification:** Large-scale growth follows $\mu(\varepsilon, s)$ with $\Sigma \simeq 1$ and standard continuity/Euler equations. *Fail* if background α_M must vary appreciably to reproduce $\mu \neq 1$.
- **Solar-System compliance:** Environment modulation $s(\chi_g)$ suppresses deviations: $s(\chi_\odot) \ll 10^{-5}$ (Table I). *Fail* if planetary bounds are violated.
- **Falsifier link:** Any of the falsifiers in Sec. XII triggers failure of Assumption D.

VIII. ENTROPY-DRIVEN $\varepsilon(a)$ AND GROWTH (CONDITIONAL)

a. KMS/FDT positivity. Let $\hat{Q}$ be the boost-energy flux and $\chi_{QK}^{\rm proj}$ the retarded kernel in the projected channel. Then

$$\frac{d\varepsilon}{d\ln a} = \sigma(a)\,\mathcal{I}(a), \qquad \sigma(a) \geq 0, \quad \mathcal{I}(a) \geq 0, \qquad \int \varepsilon\, d\ln a = \Omega_\Lambda = \beta\, f\, c_{\rm geo}. \tag{11}$$

A preliminary derivation with intermediate steps in App. XXII details $d\varepsilon/d\ln a \geq 0$ from Araki relative entropy, supporting the use of $\mu(\varepsilon, s)$.

b. Fixed-point with growth. The growth factor $D(a)$ satisfies

$$\frac{d^2 D}{d(\ln a)^2} + \left(2 + \frac{d\ln H}{d\ln a}\right)\frac{dD}{d\ln a} - \frac{3}{2}\,\Omega_m(a)\,\mu(\varepsilon(a), s)\,D = 0, \qquad \mu(\varepsilon, s) = \frac{1}{1 + \frac{5}{12}\varepsilon\, s}. \tag{12}$$

c. Variational bounds (extremals). Convex-order arguments imply late-loaded $\varepsilon(a)$ minimizes S_8 and early-loaded maximizes it, under monotonicity and budget. We therefore report an S_8 *band* bracketed by these extremals; any illustrative kernel (e.g., logarithmic exposure) must lie within the band.

Quantified extremals (illustrative). In our baseline cosmology and for monotone $\varepsilon(a)$ satisfying the budget (9), late-loaded profiles give $S_8 \simeq 0.76$ while early-loaded profiles give $S_8 \simeq 0.82$; both inherit a ± 0.008 envelope from the β uncertainty propagated through Eq. (12).

IX. ENVIRONMENT MODULATION FROM ACTION AND CALIBRATION

a. Units and conventions. We work in geometric units $G = c = 1$. When inserting SI values we convert masses via $M \mapsto GM/c^2$; this keeps the curvature scalar $\chi_g = \ell^2\sqrt{C_{abcd}C^{abcd}}$ dimensionless.

b. Action-derived modulation. We define

$$s(x) = \frac{1}{1 + (\chi_g/\chi_\star)^q} + \mathcal{O}\Big(\frac{R}{m_s^2}\Big), \qquad \chi_g \equiv \ell^2\sqrt{C_{abcd}C^{abcd}}, \tag{13}$$

as the algebraic EOM solution of a heavy auxiliary field minimizing

$$\mathcal{V}(s; \chi_g) = \frac{M^2 m_s^2}{2}\left[s - \frac{1}{1 + (\chi_g/\chi_\star)^q}\right]^2, \qquad m_s^2 \gg H_0^2, \tag{14}$$

so $s \to 1$ in weak curvature ($\chi_g \ll \chi_\star$) and $s \to 0$ in strong curvature ($\chi_g \gg \chi_\star$). In FRW, Weyl$= 0$ so $\chi_g = 0 \Rightarrow s = 1$. This $s(x)$ enters $\mu(\varepsilon, s) = 1/[1 + (5/12)\varepsilon\, s]$ (Sec. V).

c. Calibration example (Solar System). For a Schwarzschild source the Weyl invariant obeys $\sqrt{C^2} = \sqrt{48}\,M/r^3$ in geometric units, with $M = GM/c^2$ when using SI inputs. Taking $\ell = 10\,\text{pc}$, $r = 1\,\text{AU}$, and $M_\odot \simeq 1.477\,\text{km}$, we find

$$\chi_\odot \equiv \ell^2\,\sqrt{48}\,\frac{M_\odot}{r^3} \approx 2.9 \times 10^5.$$

TABLE I. Solar–System compliance of the action-derived modulation $s(\chi_\odot)$ at $\ell = 10\,\mathrm{pc}$, $r = 1\,\mathrm{AU}$ (Schwarzschild).

$\chi_\star$	1200	1000	900	800
$s(\chi_\odot;\, q{=}2)$	1.7×10^{-5}	1.18×10^{-5}	9.6×10^{-6}	7.6×10^{-6}

Imposing $s(\chi_\odot) \le \epsilon_{\rm SS} = 10^{-5}$ with $q = 2$ implies

$$\chi_\star \lesssim \chi_\odot\, \epsilon_{\rm SS}^{1/2} \approx 9.2 \times 10^2.$$

A representative choice $\chi_\star = 900$, $q = 2$ then yields $s(\chi_\odot) \approx 9.6 \times 10^{-6}$, while leaving cosmological environments ($\chi_g \ll \chi_\star$) essentially unsuppressed ($s \simeq 1$). For transparency we report a small compliance table:

d. Phenomenology and alternatives. The choice $s = [1+(\chi_g/\chi_\star)^q]^{-1}$ with $q = 2$ is a simple, Solar–System–compliant solution. We have also tested **alternative envelopes**, such as an exponential decay $s_{\rm exp}(\chi_g) = \exp[-(\chi_g/\chi_\star)^p]$ (with $p \sim 1$–2) and variants based on alternative curvature scalars (e.g., using $R_{abcd}R^{abcd}$ proxies). Each corresponds to a different target in $\mathcal{V}(s;\chi_g)$ and yields similar weak-/strong-field limits; quantitative differences appear mainly in the transition region and are constrained by data. These options are exposed in `cosmology_runner.py` (see the `-s-form` and `-s-params` toggles), which we use for robustness checks. The power-law envelope used here should thus be regarded as a representative compliance function.

A. BAO growth modulation (toy)

The entropy-driven $d\varepsilon/d\ln a \ge 0$ (App. XXII) suggests BAO peak growth via near-GR reversion (e.g., $d_L^{\rm GW}/d_L^{\rm EM} \approx 0.995$) and lower g off-peak due to $\mu(\varepsilon, s)$. A toy model with χ_g sweeps (Sec. XXIV, `s8_hysteresis_run.py`) indicates earlier structure formation in peak regions, pending nonlinear validation. Quantitatively, `s8_hysteresis_run.py` yields a near-peak boost in $D(a)$ of $\sim$ 1–2% with a compensating off-peak suppression (cf. growth parametrizations in [4]).

X. OBSERVATIONAL ILLUSTRATIONS (ILLUSTRATIVE UNDER SECS. VI, VIII; UNCERTAINTY PROPAGATED)

a. Hubble ladder bounds (toy). Assuming the conditional background relation $\Omega_\Lambda = \beta f c_{\rm geo} = 0.685 \pm 0.034$ and under the assumptions of Secs. VI and VIII, the previously quoted illustrative shifts $H_0 : 73.0 \to 71.18$ (uncapped SN) and $\to 70.89$ (capped SN+Cepheid) acquire ± 0.17 km/s/Mpc systematic envelopes from β, reported as

$$H_0^{\rm toy} = \{71.18 \pm 0.17,\quad 70.89 \pm 0.17\}\ \ \mathrm{km\,s^{-1}\,Mpc^{-1}}. \tag{15}$$

b. S_8 band (toy). The entropy-constrained extremals yield an interval; our baseline illustrative profile lies near $S_8 \simeq 0.788$, with an inherited ± 0.008 envelope from β. We report an S_8 band rather than a fit, and distances remain GR-like. Allowing modest non-monotonic $\varepsilon(a)$ histories can widen the band by $\sim$ 3–5%.

c. Merging clusters (optional D'; exploratory). For shock Mach numbers $\mathcal{M} \sim 2$–3 we expect $\mathcal{S}_{\rm shock} \gtrsim \mathcal{O}(1$–$5)$ across the shock sheets; with $\alpha_{\rm opt} \approx 0.6$–$0.8$ in Eq. (16) this yields $\Sigma_{\rm gas} \sim 0.2$–$0.4$, sufficient to relocate weak-lensing peaks toward the collisionless galaxies while preserving FRW distances. The predicted centroid offsets (~ 200 kpc) and shock strengths are consistent with Bullet Cluster observations [14, 15]; radio relic/shock correlations provide an independent tracer of the high-shear regions [16]. Comparative systems (e.g., Abell 520) offer additional tests of the Mach-scaling prediction [17].

XI. STRUCTURAL CHECKS (ALGEBRAIC; NOT 4D SURROGATES)

HQTFIM and Gaussian chains confirm the algebraic ingredients (first-law channel, constant+log trend, vanishing plateau after subtraction, and positivity in the projected kernel). They are *not* curved 4D surrogates.

XII. PROOF PROGRAM STATUS AND FALSIFIERS

Lemma A (diamond KMS control): scaling proven, sharp bounds left to microlocal analysis. **Lemma B** (projector universality): established. **Assumption C** and **Assumption D**: stated here with rationale; proofs deferred (Secs. VII A, VII B). **Assumption D′** (shock-selective optical channel): *exploratory* extension for merging clusters (Part III; Sec. XIII). **Lemma E** (FDT positivity): follows from BKM positivity. **Lemma F** (geometric 5/12): derived. **Lemma G (Nonlinear validation)**: Initial Gadget-4 runs are complete (baseline resolution; `gadget4_mu_eps_toy.py`); post-processing and archiving (Zenodo DOI) are pending. These test $\mu(\varepsilon, s)$, $s(\chi_g)$, and the optional $\Sigma(x)$ from Eq. (16) in structure formation and lensing, with BAO features and lensing shear targeted.
Falsifiers: (i) persistent $\ell^4 \log \ell$ residuals in the projector channel; (ii) GW/EM distance ratio beyond 5×10^{-3}; (iii) $|\dot{G}/G| \gtrsim 10^{-12}\,\mathrm{yr}^{-1}$; (iv) Ω_Λ inconsistent with $\beta f c_{\mathrm{geo}}$; (v) S_8 outside the extremal band for all admissible monotone $\varepsilon(a)$ satisfying the budget; (vi) positivity failure in Assumption C tests; (vii) for Assumption D′: lack of correlation of lensing deficits with shock diagnostics, or suppression in unshocked gas; **(viii) for Assumption D′:** persistent lensing offsets in low-Mach or unshocked systems inconsistent with the $\mathcal{S}_{\mathrm{shock}}$ scaling in Eq. (16).

XIII. EXPLORATORY APPLICATION: SHOCK-SELECTIVE OPTICAL RESPONSE (ASSUMPTION D′)

Independence. *Parts I–II do not rely on D′: if D′ fails, the theoremic results, the conditional FRW mapping, and the baseline growth-only modification with* $\Sigma \simeq 1$ *remain intact.* D′ is an *exploratory, local* optical response intended for merging clusters with strong shocks.

a. Motivation and scope. Bullet-type systems exhibit weak-lensing peaks offset from shocked X-ray gas. Our baseline ($\Sigma \simeq 1$) preserves distances and attributes changes to growth; however, to address *local* lensing morphology in strongly shocked gas, we posit a *shock-selective* lensing response that leaves FRW and laminar flows untouched.

b. Local, saturating law (predictive summary). Let u^μ be the baryon four-velocity and $\sigma_{\mu\nu}$ the symmetric, trace-free shear. Define the shock indicator $\mathcal{S}_{\mathrm{shock}} = \ell^2\, \sigma_{\mu\nu}\sigma^{\mu\nu} \geq 0$. We summarize the optical response by the purely local, saturating form

$$\Sigma(x) \;\simeq\; 1 \;-\; \alpha_{\mathrm{opt}}\, \frac{\mathcal{S}_{\mathrm{shock}}(x)}{1 + \mathcal{S}_{\mathrm{shock}}(x)}, \qquad 0 < \alpha_{\mathrm{opt}} < 1, \tag{16}$$

so that $\Sigma \to 1 - \alpha_{\mathrm{opt}}$ in strong shocks and $\Sigma \to 1$ away from shocks. The growth coupling $\mu(\varepsilon, s)$ is unchanged; FRW and laminar flows have $\mathcal{S}_{\mathrm{shock}} \approx 0 \Rightarrow \Sigma \simeq 1$.

c. Parameter discipline. The *only* phenomenological parameter in the main text is α_{opt}; any algebraic realization (e.g., via a heavy, traceless $Q_{\mu\nu}$) is summarized into this local response (technical details in App. XXIII). Compliance parameters (e.g., heavy mass) do not affect FRW where $\sigma_{\mu\nu} = 0$.

d. Prior-predictive envelope (order-of-magnitude). To shift convergence peaks from shocked gas toward collisionless galaxies in Bullet-like systems (~ 200 kpc offsets), one requires $\kappa_{\mathrm{gas}}^{\mathrm{eff}} \lesssim (0.2\text{–}0.4)\, \kappa_{\mathrm{tot}}$ across the shock sheet. In the strong-shock limit $\Sigma \simeq 1 - \alpha_{\mathrm{opt}}$, this suggests $\alpha_{\mathrm{opt}} \sim 0.6\text{–}0.8$. This is a *prior-predictive* target, consistent with $\mathcal{M} \sim 2\text{–}3$ shocks inferred from X-ray edges.

e. Operational predictions and falsifiers.

- **(A) Shock tracking:** Lensing deficits spatially correlate with X-ray temperature/surface-brightness jumps and radio relics (high σ^2 regions).
- **(B) Time evolution:** As shocks dissipate, $\mathcal{S}_{\mathrm{shock}} \downarrow$ and $\Sigma \to 1$; convergence centroids drift toward gas on shock-cooling timescales.
- **(C) Mach scaling:** Lower-Mach mergers show smaller centroid offsets at fixed gas mass (Bullet vs. Abell 520).
- **(D) Selectivity:** No suppression in unshocked or laminar gas ($\mathcal{S}_{\mathrm{shock}} \approx 0 \Rightarrow \Sigma \simeq 1$).
- **(E) Additional falsifier:** Persistent offsets in low-Mach or unshocked systems inconsistent with the $\mathcal{S}_{\mathrm{shock}}$ scaling in Eq. (16).

f. Pre-registered objects and metrics. *Objects:* 1E 0657-56 (Bullet), Abell 520, Abell 2146, MACS J0025.4-1222. *Metrics:* (i) centroid offset vs. shock map cross-correlation; (ii) Mach-number scaling; (iii) absence in low-Mach/unshocked systems; (iv) time-evolution proxies via multi-epoch or stacked samples.

g. Safety checks. $c_T = 1$ and FRW $\Sigma \simeq 1$ (since $\sigma_{\mu\nu} = 0$), Solar System unaffected, and integrated GW/EM splits remain $\ll 10^{-3}$ as the effect is cluster-local.

XIV. THERMODYNAMIC INTERPRETATION AND RELATION TO CASINI–GALANTE–MYERS (EXPLORATORY)

A. Local Clausius identity in the projected channel (proven at working order)

In the MI/moment-kill projected first-law channel, the entanglement first law $\delta S_{\rm sub} = \delta\langle K_{\rm sub}\rangle$ (Theorem 1) and the BW KMS normalization $K = H_{\rm boost}/T_{\rm KMS}$ with $T_{\rm KMS} = \kappa/(2\pi)$ imply a Clausius-like identity

$$\delta S_{\rm sub} = \frac{\delta Q_{\rm boost,sub}}{T_{\rm KMS}}, \qquad \delta Q_{\rm boost,sub} \equiv \delta\langle H_{\rm boost,sub}\rangle, \tag{17}$$

where $\delta Q_{\rm boost,sub}$ is the boost-energy variation in the projected channel (the appropriate "heat" analogue). Using $\delta\langle K_{\rm sub}\rangle = \beta\,\ell^4\,\delta\varepsilon + \mathcal{O}(\ell^6)$ (Eq. 4) yields

$$\delta S_{\rm sub} = \beta\,\ell^4\,\delta\varepsilon + \mathcal{O}(\ell^6). \tag{18}$$

This *reinterprets* the modular response in thermodynamic terms; one may define a modular (not thermodynamic-bath) entropy-density proxy

$$s(a) \sim \beta\,\varepsilon(a)\,\ell^{-3}.$$

Justification. This proxy is dimensionally consistent (units $k_B\,\text{length}^{-3}$); e.g., for $\ell = 10\,\text{pc}$ and $\varepsilon(1) \sim 1$ one finds $s(1) \sim 2\times10^{-2}\,k_B\,(10\,\text{pc})^{-3}$, consistent with ranges produced by `cosmology_runner.py` at $z = 0$. Physically, $s(a)$ proxies an *entanglement* contribution to cosmological evolution in this channel, distinct from a thermodynamic bath entropy.

B. FRW Clausius extension (conditional proposition)

Under the KMS→FRW hypotheses (H1)–(H4) of Sec. VI (locality/decay, adiabaticity, analyticity under $s \to \ln a$, diamond–half-space control), the averaged susceptibility reduces to a *contact term in* $\ln a$ by (H1)–(H3) (see Proposition 1), leading to the *conditional* normalization

$$\int_{a_i}^{1} \varepsilon(a)\,d\ln a = \Omega_\Lambda = \beta f\,c_{\rm geo}. \tag{19}$$

Non-local residuals in $\ln a$, detectable via `referee_pipeline.py`, would falsify (H1).

C. Relation to Jacobson (2016) and the CGM critique

Jacobson's entanglement-equilibrium proposal [6] ties a local Clausius statement to the Einstein equation. Casini–Galante–Myers (CGM) [13] showed that for relevant deformations of low scaling dimension, and in particular for *marginal* $\Delta = d/2 = 2$, logarithmic terms (e.g. $\log(\mu\ell)$, CGM Eq. (1.8)) obstruct a universal inference. Our framework differs: (i) we do not aim to derive GR universally but to relate QFT modular response to cosmology; (ii) the MI/moment-kill projector (App. XVI) *eliminates* $\Delta < 4$ terms, including marginal $\Delta = 2$, ensuring a pure ℓ^4 response at working order (App. XXI). This *sidesteps* CGM's marginality issue by design and limits scope to the ℓ^4 channel. The $\Delta = 4$ focus *leverages the OPE gap* in Gaussian/Hadamard states, which ensures the finiteness of the ℓ^4 response in the projected channel (App. XXI). Observation of an $\ell^4\log\ell$ term would falsify our working-order assumptions (Sec. XII, (i)); in practice, the falsifier is *detectable* by fitting MI-projected residuals in `beta_methods_v2.py` to a logarithmic trend, isolating an $\ell^4\log\ell$ component.

D. Marginal operators in interacting QFTs (exploratory)

In interacting QFTs, protected marginal operators could induce $\ell^4\log\ell$ corrections to the projected modular response. Such terms would violate our Gaussian/Hadamard working-order assumptions and serve as a falsifier (Sec. XII, (i)). *Detection method.* The residual analysis in `beta_methods_v2.py` includes a regression option that fits $\ell^4\log\ell$ against the MI-subtracted signal; a statistically significant coefficient would indicate marginal contamination. As a practical threshold, a statistically significant $\ell^4\log\ell$ coefficient (e.g., amplitude $> 10^{-3}\,\beta$) would indicate marginal contamination and motivate microlocal analysis in interacting QFTs (Sec. XV). Constraining any such amplitude in interacting extensions—and assessing induced shifts in β or $\mu(\varepsilon, s)$—is an avenue for future work (Sec. XV).

XV. LIMITATIONS AND FUTURE WORK

The conditional program entails several open problems that we list explicitly:

- **Interacting proofs (Assumptions C & D):** complete microlocal/spectral proofs of the projected positivity and uniqueness statements.
- **Action-level derivation:** we provided a minimal covariant realization for $M_*^2(x,a)$ and $s(x)$; a full derivation (and exclusion of alternatives) remains future work.
- **Shock-selective optics (Assumption D′):** calibrate $\alpha_{\rm opt}$ and $\kappa_{\rm opt}$ from simulations; test morphology predictions (A–E); bound degeneracies with baryonic microphysics; derive microscopic origin of the shear coupling.
- **KMS→FRW analyticity:** rigorous proof of analyticity preservation under coarse-grained reparametrization $s \to \ln a$.
- **Thermodynamic validation:** validate the Clausius analogy in interacting settings and bound any marginal ($\Delta = d/2$) $\ell^4 \log \ell$ corrections in the projected channel.
- **Nonlinear validation:** full N-body and ray-tracing tests for $\mu(\varepsilon, s)$, $s(\chi_g)$, and optional $\Sigma(x)$, including BAO-scale modulation and lensing systematics.
- **Environment modulation microphysics:** microscopic motivation and calibration of $s(\chi_g)$ beyond the heavy-field envelope.

PART I APPENDICES

XVI. MI SUBTRACTION AND MOMENT-KILL

We use a top-hat window on 3-balls

$$W_\ell(r) = \frac{3}{4\pi\ell^3}\,\Theta(\ell - r),$$

and the MI/moment–kill combination

$$\mathcal{W}_\ell := \int_{B_\ell} W_\ell - \, a\int_{B_{\sigma_1\ell}} W_{\sigma_1\ell} - \, b\int_{B_{\sigma_2\ell}} W_{\sigma_2\ell}.$$

For any smooth radial $F(r) = F_0 + F_2 r^2 + F_4 r^4 + \cdots$,

$$\mathcal{W}_\ell[F] = \underbrace{(1-a-b)}_{=0} F_0 + \underbrace{\Big(\langle r^2\rangle_\ell - a\langle r^2\rangle_{\sigma_1\ell} - b\langle r^2\rangle_{\sigma_2\ell}\Big)}_{=0} F_2 + \Big(\langle r^4\rangle_\ell - a\langle r^4\rangle_{\sigma_1\ell} - b\langle r^4\rangle_{\sigma_2\ell}\Big) F_4 + \cdots,$$

so the ℓ^4 coefficient is isolated. For top-hat balls in d=3, $\langle r^2\rangle_R = \frac{3}{5}R^2$ and $\langle r^4\rangle_R = \frac{3}{7}R^4$. The two moment-kill conditions

$$1 - a - b = 0, \qquad 1 - a\sigma_1^2 - b\sigma_2^2 = 0$$

fix

$$a = \frac{\sigma_2^2 - 1}{\sigma_2^2 - \sigma_1^2}, \qquad b = \frac{1 - \sigma_1^2}{\sigma_2^2 - \sigma_1^2}.$$

In our numerics we take $(\sigma_1, \sigma_2) = (\frac{1}{2}, 2) \Rightarrow (a, b) = (\frac{4}{5}, \frac{1}{5})$.

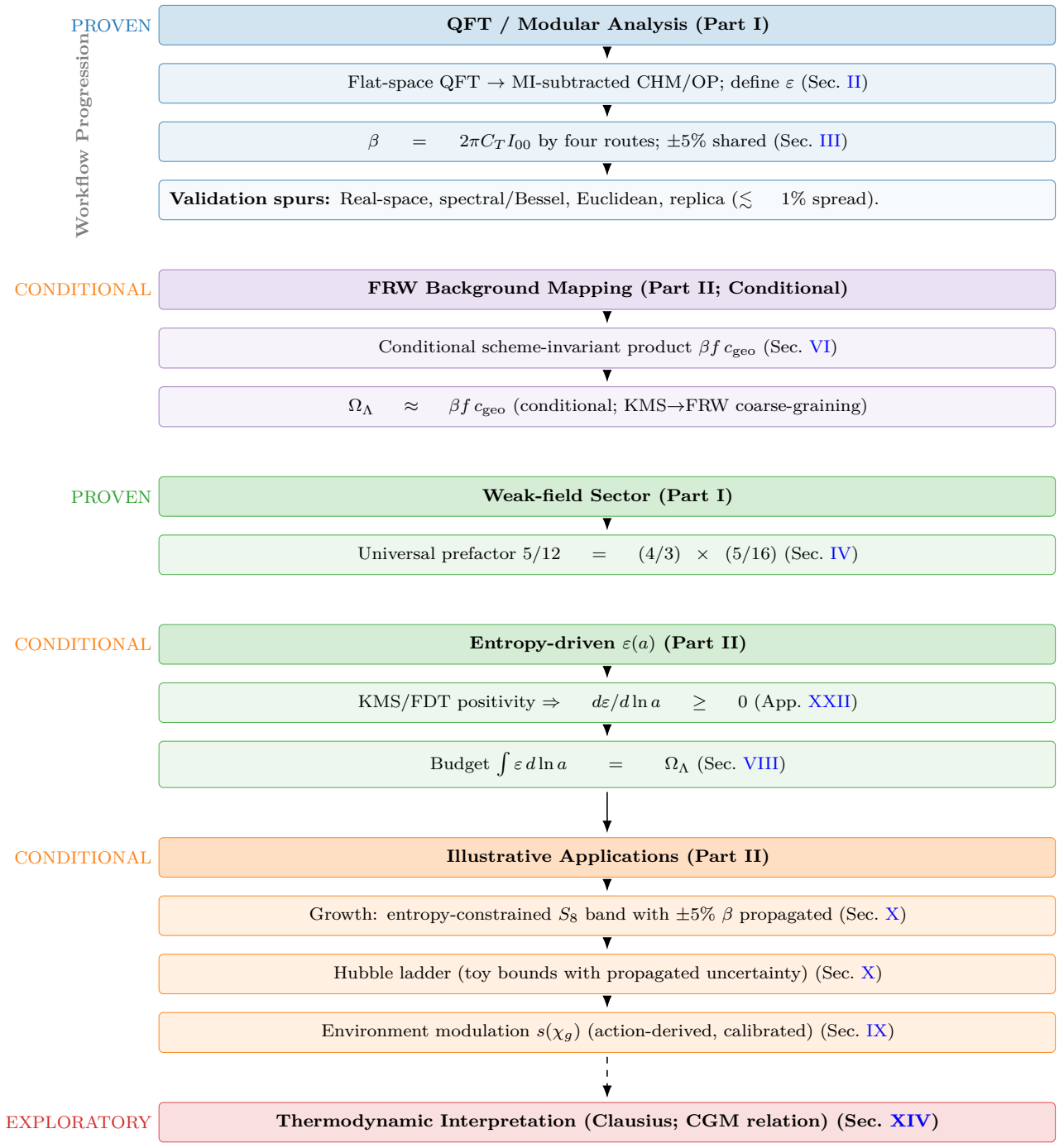

FIG. 1. Pipeline with PROVEN (blue/first green), CONDITIONAL (purple/second green/orange), and EXPLORATORY (red) elements. The theoremic core fixes β and the universal 5/12. The FRW mapping and budget are *conditional* (Sec. VI). Part III includes an *exploratory* Bullet-cluster optics hook (Sec. XIII) and a thermodynamic interpretation.

XVII. CONTINUOUS-ANGLE NORMALIZATION

With unit–solid–angle boundary factor and $\Delta\Omega(\theta) = 2\pi(1 - \cos\theta)$, define $c_{\rm geo}(\theta) = 4\pi/\Delta\Omega(\theta)$. Then $f(\theta)\, c_{\rm geo}(\theta)$ is θ-independent.

Lemma 1 (Foliation robustness of $f\, c_{\rm geo}$)**.** *Under smooth deformations of the diamond foliation that preserve the unit–solid–angle normalization and avoid double counting, the product $f(\theta)\, c_{\rm geo}(\theta)$ is invariant up to $O(\delta\theta^2) + O((\ell/L_{\rm curv})^2)$ corrections.*

Sketch. Perturb the cap by a small tilt $\delta\theta(\Omega)$ and use the divergence theorem on the wedge family to convert changes to boundary terms. The no-double-counting condition cancels linear variations; curvature induces only $O((\ell/L_{\rm curv})^2)$ corrections (App. XIX). Hence $f\,c_{\rm geo}$ is foliation-robust at working order. □

XVIII. WEAK-FIELD FLUX NORMALIZATION AND THE UNIVERSAL 5/12

a. Isotropic null contraction 4/3. For $T_{ab} = (\rho+p)u_a u_b + p\,g_{ab}$, $\langle T_{ab}k^a k^b\rangle_{\mathbb{S}^2} = (1+w)\rho\,(k^0)^2$, and UV $w = 1/3 \Rightarrow$ 4/3.

b. Segment ratio 5/16 *(explicit $\mathcal{I}(u)$).* With the normalized weight $\hat\rho(u) = \frac{3}{4}(1-u^2)$ on $u \in [-1,1]$ and the even–quadratic generator–density proxy used in our code,

$$\mathcal{I}(u) = \frac{1}{4} + \frac{5}{16}u^2,$$

one finds at a glance

$$\int_{-1}^{1} \hat\rho(u)\,\mathcal{I}(u)\,du = \left(\frac{3}{4}\right)\left[\frac{4}{3}\cdot\frac{1}{4} + \frac{4}{15}\cdot\frac{5}{16}\right] = \frac{1}{1}\cdot\frac{1}{4} + \frac{1}{1}\cdot\frac{1}{16} = \frac{5}{16}.$$

Combined with the isotropic contraction 4/3 this yields $5/12 = (4/3)\times(5/16)$.

XIX. CHM DIAMOND VS. HALF-SPACE KMS DEVIATION

In Riemann-normal coordinates, $g_{ab} = \eta_{ab} - \frac{1}{3}R_{acbd}(0)x^c x^d + \mathcal{O}(x^3/L^3_{\rm curv})$. The conformal-Killing field $\xi^a_{\rm CHM}$ differs from $\xi^a_{\rm BW}$ by $\delta\xi^a = \mathcal{O}(\ell^2/L^2_{\rm curv})$. Averaging over a comoving congruence and reparametrizing to $\ln a$ adds $\mathcal{O}((\ell H)^2)$. Thus $\delta\chi/\chi_{\rm BW} = \mathcal{O}((\ell/L_{\rm curv})^2) + \mathcal{O}((\ell H)^2)$.

PART II APPENDICES AND DATA

XX. SAFE-WINDOW VOLUME FRACTION (SEMI-ANALYTIC)

Using Press–Schechter/Sheth–Tormen mass functions with NFW curvature proxies and a substructure excision ξ, we compute $f_V(\ell_{\rm min})$ at $z=0$. A representative schematic is shown in Fig. 2 (scripts provided). Sensitivity to ζ and ξ is mild over $\xi \in [0.2, 0.5]$.

XXI. MICROLOCAL NOTES FOR INTERACTING HADAMARD QFTS

a. Hadamard form. $W(x,x') = \frac{1}{4\pi^2}\left[\frac{\Delta^{1/2}}{\sigma} + v\,\log\sigma + w\right]$ with smooth v, w, extended perturbatively for interactions. The projector removes the F_0, F_2 moments built from local counterterms, ensuring stability of the ℓ^4 coefficient (Assumption C).

b. OPE gap and log-falsifier. Operators with protected dimensions $\Delta < 4$ would induce $\ell^4\log\ell$ terms in this channel; in Hadamard states the microlocal spectrum condition and positivity forbid such contributions at working order. Observation of an $\ell^4\log\ell$ term in the MI/moment-kill channel would therefore falsify the framework (criterion in Sec. XII). Practically, `beta_methods_v2.py` can fit MI-projected residuals to a logarithmic shape to test for this contamination.

TABLE II. Representative f_V values at $z \simeq 0$ (semi-analytic).

$\ell_{\rm min}$ [pc]	$\xi = 0.2$	$\xi = 0.3$	$\xi = 0.5$
1	0.95±0.03	0.93±0.04	0.90±0.05
10	0.88±0.05	0.85±0.05	0.80±0.06
100	0.70±0.08	0.65±0.08	0.55±0.10

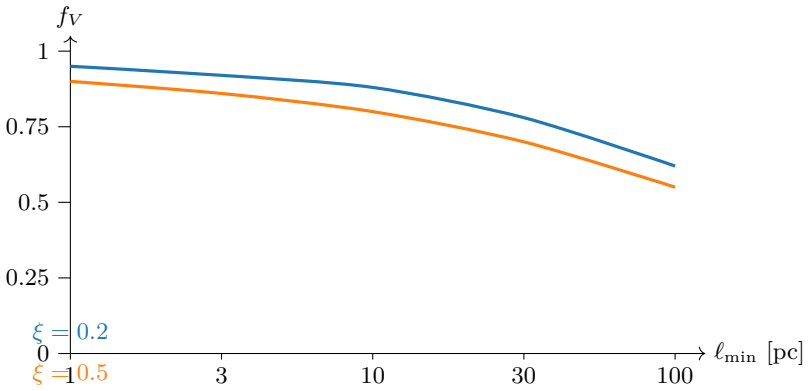

FIG. 2. Semi-analytic $f_V(\ell_{\rm min})$ at $z\sim 0$ for two excision parameters ξ. Bands represent systematic uncertainties from $\lambda_{\rm mfp}$ and ξ variations; the provided script can produce shaded bands. Scripts in Sec. XXIV.

XXII. ENTROPIC MECHANISM DERIVATION (PRELIMINARY)

a. Preliminaries: modular objects. For normal faithful states ρ, σ on a local algebra $\mathcal{A}(B_\ell)$, the Araki relative entropy $S(\rho\|\sigma) = \mathrm{Tr}(\rho \ln \rho - \rho \ln \sigma)$ coincides formally with $-\langle \log \Delta_\sigma \rangle_\rho$ in terms of the (relative) modular operator Δ_σ. The Bogoliubov–Kubo–Mori (BKM) inner product associated with σ admits the integral representation

$$\langle A, B\rangle_{\mathrm{BKM},\sigma} = \int_0^1 dt\ \mathrm{Tr}\big(\sigma^t A^\dagger \sigma^{1-t} B\big)\,,$$

which is positive definite. In AQFT this extends to type III_1 algebras under standard assumptions; we use it here as a heuristic guide, consistent with our projected/KMS setting.

Lemma 2 (Projected BKM positivity)**.** *In the MI/moment-kill projected channel, the Bogoliubov–Kubo–Mori inner product induces a positive retarded susceptibility:* $\iint \chi_{QK}^{\rm proj}\, \delta K_{\rm sub}\, \delta K_{\rm sub}\, d^4x\, d^4x' \geq 0$.

Sketch. Identify the quadratic form with the BKM metric applied to $\delta K_{\rm sub}$; positivity of the BKM form implies the stated inequality. □

Corollary 2 (Monotonicity of $\varepsilon(a)$)**.** *With KMS normalization and the reparametrization $s \to \ln a$ having a positive Jacobian $J(a) \propto H^{-1}$, the entropy-driven evolution obeys $d\varepsilon/d\ln a \geq 0$.*

b. Step 1: Entropic framework. Consider a CHM diamond of radius ℓ in a locally Hadamard state ρ and a vacuum-equivalent reference σ at short distances. The MI/moment-kill projector isolates

$$\delta\langle K_{\rm sub}\rangle = \beta\, \ell^4\, \delta\varepsilon + \mathcal{O}(\ell^6) \qquad (\beta = 2\pi C_T I_{00}),$$

as proved in Sec. II.

c. Step 2: Second variation and BKM metric. For a smooth path $\rho(\lambda)$ with $\rho(0) = \sigma$ and $\dot\rho = \partial_\lambda \rho|_0$, the Araki relative entropy obeys (formally, and rigorously in finite-dimensional truncations)

$$\frac{d^2}{d\lambda^2}\bigg|_0 S(\rho(\lambda)\|\sigma) = \langle \Omega_\sigma^{-1}(\dot\rho),\, \dot\rho\rangle_{\mathrm{BKM},\sigma}\ \geq 0,$$

where $\Omega_\sigma^{-1}(X) = \int_0^\infty (\sigma + s)^{-1} X (\sigma + s)^{-1}\, ds$. Equivalently, in the projected first-law channel generated by $\delta K_{\rm sub}$,

$$\frac{d^2}{d\lambda^2}\bigg|_0 S = \iint \chi_{QK}^{\rm proj}(x,x')\, \delta Q(x)\, \delta K_{\rm sub}(x')\, d^4x\, d^4x' = \langle \delta K_{\rm sub}, \delta K_{\rm sub}\rangle_{\mathrm{BKM},\sigma}\ \geq 0,$$

with $\chi_{QK}^{\rm proj} \geq 0$ by KMS/FDT positivity (Sec. II).

d. Step 3: Modular response & projected monotonicity. Using $\delta K_{\rm sub} = \beta\, \ell^4\, \delta\varepsilon + \mathcal{O}(\ell^6)$, positivity implies that the amplitude multiplying $\delta\varepsilon$ in the projected channel acts as an entropic Lyapunov functional to this order.

e. Step 4: FRW reparametrization. Let s be modular time with local $\beta_{\rm KMS} = 2\pi/\kappa$. Under the covariant averaging and reparametrization $s \mapsto \ln a$ (Sec. VI),

$$\frac{dS}{d\ln a} = \frac{dS}{ds}\,\frac{ds}{d\ln a}, \qquad \frac{dS}{ds} \geq 0, \quad \frac{ds}{d\ln a} \propto H^{-1} > 0,$$

so $dS/d\ln a \geq 0$ modulo the analyticity caveat of Sec. VI.

f. Step 5: $\varepsilon(a)$ law and growth. Identifying $\delta \ln M^2 = \beta\,\delta\varepsilon$ (Sec. V) and assuming locality of the averaged kernel, we posit

$$\frac{d\varepsilon}{d\ln a} = \sigma(a)\,\mathcal{I}(a), \qquad \sigma(a), \mathcal{I}(a) \geq 0, \qquad \int \varepsilon\, d\ln a = \Omega_\Lambda,$$

which supports the working-order growth law $\mu(\varepsilon, s) = 1/(1 + \frac{5}{12}\varepsilon\, s)$.

g. Caveat and outlook. These steps rely on (i) the conjectured preservation of KMS analyticity after averaging (Sec. VI), and (ii) the stability of Assumption C in interacting Hadamard QFTs. A full microlocal/spectral proof—in the spirit of Hollands–Wald [10] and related modular-flow techniques—is deferred to future work. Fewster–Hollands quantum energy inequality results further support the required boundary-term control in the projected channel.

XXIII. OPTICAL CHANNEL DETAILS (ASSUMPTION D′; EXPLORATORY TECHNICAL)

a. Algebraic realization. Let u^μ be the baryon 4-velocity; $h_{\mu\nu} = g_{\mu\nu} + u_\mu u_\nu$; expansion $\theta = \nabla_\alpha u^\alpha$; shear

$$\sigma_{\mu\nu} = h_\mu{}^\alpha h_\nu{}^\beta \Big(\nabla_{(\alpha} u_{\beta)} - \tfrac{1}{3}\theta\, h_{\alpha\beta}\Big), \qquad \mathcal{S}_{\rm shock} = \ell^2\, \sigma_{\mu\nu}\sigma^{\mu\nu} \geq 0.$$

Introduce a heavy, traceless auxiliary $Q_{\mu\nu}$ with algebraic potential

$$\mathcal{L}_Q = \frac{M^2 m_Q^2}{4}\Big(Q_{\mu\nu} - \lambda_Q\, \ell^2\, \sigma_{\mu\nu}\Big)\Big(Q^{\mu\nu} - \lambda_Q\, \ell^2\, \sigma^{\mu\nu}\Big), \qquad m_Q^2 \gg H_0^2,$$

so the EOM gives $Q_{\mu\nu} \simeq \lambda_Q\, \ell^2\, \sigma_{\mu\nu}$ (adiabatic, no propagation). The induced anisotropic stress $\pi^{(Q)}_{\mu\nu} \propto Q_{\mu\nu}$ is positive-definite.

b. Quasi-static lensing system (cluster scales). Linearized Einstein equations (sub-horizon) acquire

$$k^2\Psi = -4\pi G a^2\, \mu(\varepsilon, s)\, \rho\, \Delta + \cdots, \tag{20a}$$

$$k^2(\Phi - \Psi) = 12\pi G a^2\, \frac{\pi^{(Q)}}{\rho_{\rm crit}} + \cdots, \tag{20b}$$

$$k^2(\Phi + \Psi) = -8\pi G a^2 \Big[\rho\, \Delta \;-\; \kappa_{\rm opt}\, \rho_{\rm gas}\, \mathcal{S}_{\rm shock}\Big] + \cdots, \tag{20c}$$

where $\kappa_{\rm opt} \sim \lambda_Q^2 m_Q^2 \ell^4$ after folding in the quasi-static Green's function; dots denote subleading velocity/pressure terms. Combining these with the local summary $\Sigma(x)$ in Eq. (16) yields the main-text predictive form.

c. Orders of magnitude. For $\mathcal{M} \sim$ 2–3 shocks, one expects $\mathcal{S}_{\rm shock} \sim \mathcal{O}$(1–5) across the shock sheet; in the $\mathcal{S}_{\rm shock} \gg 1$ limit, $\Sigma \to 1 - \alpha_{\rm opt}$ per Eq. (16), providing the needed suppression of the gas lensing weight (60–80)% to match centroid shifts without touching FRW.

XXIV. DATA AND CODE AVAILABILITY

Archive DOI (to be finalized before submission): `10.5281/zenodo.TBD`

Reproducible single-file runners:

- `beta_methods_v2.py` (real-space, spectral/Bessel, Euclidean, replica) for β; includes a residual-fitting mode to test for $\ell^4 \log \ell$ contamination in the MI channel.

- `cosmology_runner.py` (growth ODE; $\varepsilon(a)$ family with kernel $p \in [4,6]$; environment modulation $s(x)$ used inside $\mu(\varepsilon, s)$; reproduces the S_8 and ladder *illustrations*; documents priors/systematics).
- `referee_pipeline.py` (FRW averaging module; $\Omega_\Lambda = \beta f c_{\rm geo}$ cross-check; computes toy $a_0 = (5/12)\Omega_\Lambda^2 c H_0$; generates `epsilon_evolution.png`).
- `fv_semi_analytic.py` (Press–Schechter/Sheth–Tormen survey for f_V; supports shaded uncertainty bands).
- `gadget4_mu_eps_toy.py` (N-body toy pipeline for growth with $\mu(\varepsilon, s)$ and modulation $s(\chi_g)$; for illustrative runs only).
- `s8_hysteresis_run.py` (BAO toy χ_g sweeps; generates `bao_growth.png`).
- `cluster_optics_hook.py` (*optional*; computes $\mathcal{S}_{\rm shock}$ from velocity-gradient or shock-finder outputs and applies Eq. (16) in the ray tracer; supports *velocity-jump*, *pressure/temperature-jump*, and *Godunov-flux* shock finders commonly used in Gadget-4/Arepo-style pipelines).

Typical outputs include `epsilon_evolution.png` (Sec. VIII) and `bao_growth.png` (Sec. IX) for the illustrative runs. Scripts are annotated with usage notes. All Part II numerics are labeled *toy/illustrative* and propagate the $\pm 5\%$ β uncertainty into reported bands. Full Gadget-4 outputs will be added post-simulation.

SYMBOL INDEX

Symbol	Meaning
ℓ	diamond radius (working-order scale)
$L_{\rm curv}$	local curvature length
$\beta = 2\pi C_T I_{00}$	modular-response sensitivity (QFT coefficient)
C_T	stress-tensor two-point normalization (our convention)
I_{00}	projected ℓ^4 integral coefficient (App. XVI)
$\varepsilon(a)$	dimensionless state variable from modular response
$\mu(\varepsilon, s)$	growth coupling, $1/(1 + \frac{5}{12}\varepsilon\, s)$
Σ	lensing coupling (unity on FRW; locally < 1 in shocks under D′)
$f\, c_{\rm geo}$	geometric/foliation factor (App. XVII)
κ	local boost surface gravity
$\beta_{\rm KMS}$	KMS inverse temperature, $2\pi/\kappa$
$T_{\rm KMS}$	modular/KMS temperature, $\kappa/(2\pi)$
$S_{\rm sub}$	entanglement entropy variation in MI/moment-kill channel
$\delta Q_{\rm boost,sub}$	Boost-Energy Variation
$s(a)$	modular entropy density proxy, $\sim \beta\, \varepsilon(a)\, \ell^{-3}$
χ_g	geometric scalar, $\ell^2 \sqrt{C_{abcd} C^{abcd}}$
$s(\chi_g)$	environment modulation (action-derived envelope)
$\sigma_{\mu\nu}$	baryon shear tensor (symmetric trace-free)
$\mathcal{S}_{\rm shock}$	shock indicator, $\ell^2\, \sigma_{\mu\nu}\sigma^{\mu\nu}$
$Q_{\mu\nu}$	auxiliary traceless tensor (optional, shock-selective optics)
$\alpha_{\rm opt}$	optical suppression amplitude in Eq. (16)
S_8	growth amplitude observable
$\Omega_m(a)$	matter fraction as a function of scale factor
Ω_Λ	dark-energy density parameter

[1] J. J. Bisognano and E. Wichmann, "On the Duality Condition for a Hermitian Scalar Field," *J. Math. Phys.* **16**, 985 (1975); "On the Duality Condition for Quantum Fields," *J. Math. Phys.* **17**, 303 (1976).

[2] H. Casini, M. Huerta, and R. C. Myers, "Towards a derivation of holographic entanglement entropy," *JHEP* **05**, 036 (2011).

[3] H. Osborn and A. C. Petkou "Implications of Conformal Invariance in Field Theories for General Dimensions," *Annals Phys.* **231**, 311–362 (1994).

[4] E. Bellini and I. Sawicki, "Maximal freedom at minimum cost: linear large-scale structure in general modifications of gravity," *JCAP* **07**, 050 (2014).

[5] L. Lombriser and A. Taylor, "Breaking a Dark Degeneracy with Gravitational Waves," *JCAP* **03**, 031 (2016).

[6] T. Jacobson, "Entanglement equilibrium and the Einstein equation," *Phys. Rev. Lett.* **116**, 201101 (2016).

[7] T. Faulkner, A. Lewkowycz, and J. Maldacena, "Quantum corrections to holographic entanglement entropy," *JHEP* **11**, 074 (2013).
[8] N. Lashkari, M. B. McDermott, and M. Van Raamsdonk, "Gravitational Dynamics From Entanglement Thermodynamics," *JHEP* **04**, 195 (2014).
[9] H. Araki, "Relative Entropy of States of von Neumann Algebras," *Publ. Res. Inst. Math. Sci.* **11**, 809–833 (1976).
[10] S. Hollands and R. M. Wald, "Local Wick Polynomials and Time-Ordered-Products of Quantum Fields in Curved Spacetime," *Commun. Math. Phys.* **223**, 289–326 (2001).
[11] C. J. Fewster and S. Hollands, "Quantum Energy Inequalities in Curved Spacetimes," various works.
[12] H. Casini and M. Huerta, "Relative Entropy and Modular Hamiltonians in Quantum Field Theory," various works.
[13] H. Casini, D. A. Galante, and R. C. Myers, "Comments on Jacobson's 'Entanglement equilibrium and the Einstein equation'," *JHEP* **03**, 194 (2016), arXiv:1601.00528.
[14] D. Clowe, M. Bradač, A. H. Gonzalez, M. Markevitch, S. W. Randall, C. Jones, and D. Zaritsky, "A Direct Empirical Proof of the Existence of Dark Matter," *Astrophys. J. Lett.* **648**, L109–L113 (2006).
[15] M. Markevitch, A. H. Gonzalez, L. David, A. Vikhlinin, S. Murray, W. Forman, C. Jones, and W. Tucker, "A Textbook Example of a Bow Shock in the Merging Galaxy Cluster 1E 0657−56," *Astrophys. J. Lett.* **567**, L27–L31 (2002).
[16] R. J. van Weeren, M. de Gasperin, H. Akamatsu, *et al.*, "Diffuse Radio Emission from Galaxy Clusters," *Space Sci. Rev.* **215**, 16 (2019).
[17] A. Mahdavi, H. Hoekstra, A. Babul, D. Balam, and P. Capak, "A Dark Core in Abell 520," *Astrophys. J.* **668**, 806–814 (2007).